Bifurcations in the theory of current transfer to cathodes of DC discharges and observations of transitions between different modes

Cite as: Phys. Plasmas **25**, 042307 (2018); https://doi.org/10.1063/1.5024383
Submitted: 31 January 2018 • Accepted: 05 April 2018 • Published Online: 30 April 2018

M. S. Bieniek, D. F. N. Santos, P. G. C. Almeida, et al.

Bifurcations in the theory of current transfer to cathodes of DC discharges and observations of transitions between different modes

M. S. Bieniek, D. F. N. Santos, P. G. C. Almeida, and M. S. Benilov[a)]
Departamento de Física, Faculdade de Ciências Exatas e da Engenharia, Universidade da Madeira, Largo do Município, 9000 Funchal, Portugal and Instituto de Plasmas e Fusão Nuclear, Instituto Superior Técnico, Universidade de Lisboa, 1041 Lisboa, Portugal

(Received 31 January 2018; accepted 5 April 2018; published online 30 April 2018)

General scenarios of transitions between different spot patterns on electrodes of DC gas discharges and their relation to bifurcations of steady-state solutions are analyzed. In the case of cathodes of arc discharges, it is shown that any transition between different modes of current transfer is related to a bifurcation of steady-state solutions. In particular, transitions between diffuse and spot modes on axially symmetric cathodes, frequently observed in the experiment, represent an indication of the presence of pitchfork or fold bifurcations of steady-state solutions. Experimental observations of transitions on cathodes of DC glow microdischarges are analyzed and those potentially related to bifurcations of steady-state solutions are identified. The relevant bifurcations are investigated numerically and the computed patterns are found to conform to those observed in the course of the corresponding transitions in the experiment. *Published by AIP Publishing.*
https://doi.org/10.1063/1.5024383

I. INTRODUCTION

Luminous spots on electrodes of direct current glow and arc discharges and self-organized patterns of spots represent a very interesting phenomenon, which is also important for applications. The presence, or not, of spots on electrodes is a key point for the operation of any arc device. Self-organized patterns appearing on cathodes of DC glow microdischarges are sources of excimer radiation.[1,2] Self-organized patterns on liquid anodes of atmospheric pressure glow microdischarges have been shown to produce a nontrivial cancer-inhibiting effect.[3]

The theoretical description of spots and spot patterns on electrodes of DC glow and arc discharges is based on the multiplicity of solutions: an adequate theoretical model must in some cases allow multiple steady-state solutions to exist for the same conditions (in particular, for the same discharge current I), with different solutions describing the spotless (diffuse) mode of current transfer and modes with different spot configurations.

Some of the multiple solutions may merge, or become identical at certain values of the control parameter; a bifurcation, or branching, of solutions. Bifurcations of different kinds of steady-state solutions have been encountered in the theory and modelling of current transfer to cathodes of DC glow and high-pressure arc discharges.[4,5] An understanding of these bifurcations is crucial for the computation of the whole pattern of multiple solutions and an analysis of their stability.

The existence of multiple solutions and their bifurcations, in the case of current transfer to cathodes of DC glow discharges, is a consequence of a strong positive feedback, which originates from the increasing dependence of the rate of ionization on electric field.[5] In the case of current transfer to cathodes of arc discharges, the existence of multiple solutions and their bifurcations is a result of a strong positive feedback originating from the dependence of the density of the energy flux from the plasma to the cathode surface on the surface temperature.[5] In contrast, multiple steady-state solutions describing different modes of current transfer to anodes of glow microdischarges computed recently[6] do not reveal bifurcations. The existence of multiple solutions in this case is related to the change of sign of the anode sheath voltage. Thus, the existence, or not, of bifurcations of steady-state solutions, describing different modes of current transfer to electrodes of DC glow and arc discharges, is related to the underlying physics and is therefore of significant interest.

Unfortunately, the question of whether bifurcations exist has not been addressed in experimental publications. (Although there are interesting results concerning bifurcations in the pattern of oscillations developing in a DC-driven semiconductor-gas discharge system;[7] see also Refs. 8 and 9 and review 10). It is therefore of interest to analyze available experimental observations of different modes of current transfer to electrodes of DC glow and arc discharges with the aim to eventually identify bifurcations.

The outline of the paper is as follows. In Sec. II, the general scenarios of changes between modes on electrodes of DC gas discharges and their relation to bifurcations of steady-state solutions are analyzed. Transitions of modes on cathodes of arc and DC glow, discharges are considered in Secs. III and IV, respectively. The conclusions are summarized and directions of future work are discussed in Sec. V.

II. SCENARIOS OF TRANSITIONS BETWEEN DIFFERENT MODES OF CURRENT TRANSFER TO ELECTRODES OF DC DISCHARGES AND THEIR RELATION TO BIFURCATIONS

Bifurcations of steady-state solutions manifest in experiments as transitions between modes with different spot patterns, which occur as the discharge current I is varied.

[a)]Email: benilov@uma.pt

One can distinguish two scenarios for transitions between modes with different spot patterns. First, there are quasi-stationary, i.e., continuous, and, consequently, reversible transitions between states where distributions of luminosity over the electrode surface possess different symmetries. Second, there are transitions that occur abruptly even for very small variations of I. Let us consider first the quasi-stationary transitions. All parameters of the discharge, including the discharge voltage U, vary with I continuously. In particular, the measured current-voltage characteristic (CVC) $U(I)$ is continuous. However, $U(I)$ is not smooth at $I = I_0$, where I_0 is the value of I where the distribution of luminosity over the electrode surface changes its symmetry. This transition is caused by a symmetry-breaking bifurcation that occurs at $I = I_0$, with stable states existing on both sides of the bifurcation point.

The above scenario may be illustrated by the following example. If the discharge vessel is axially symmetric, then the mathematical problem describing steady-state current transfer to the electrode admits an axially symmetric (2D) solution, describing the spotless mode of current transfer, and a 3D solution, describing a mode with a spot. (More precisely, there is a family of 3D solutions which differ one from the other by the azimuthal position of the spot. Other families of 3D solutions, describing modes with several spots, may exist as well.) It is a usual situation that the 3D spot-mode solution branches off from the 2D spotless-mode solution, a breaking-of-axial-symmetry bifurcation. In terms of the bifurcation theory, a symmetry breaking represents a pitchfork bifurcation. Note that a brief summary of information from the bifurcation theory relevant to this work can be found in Appendix of Ref. 4; a further discussion can be found, e.g., in reviews 5 and 11.

Let us designate by I_0 the value of discharge current at which the bifurcation occurs and assume for definiteness that the 2D solution is stable for $I > I_0$ and unstable for $I < I_0$. It may happen that the 3D solution branches off into the range $I < I_0$, where the 2D solution is unstable [Fig. 1(a)]. This is the so-called supercritical bifurcation. According to the general trends of the bifurcation theory, the 3D solution is stable (at least) in the vicinity of the state $I = I_0$ in this case. If such a situation is investigated experimentally and I in the experiment exceeds I_0, the discharge will operate in the 2D spotless mode and the luminosity distribution over the electrode surface will be axially symmetric. As I is reduced down to values below I_0, the luminosity distribution starts deviating from being axially symmetric and the deviation grows proportionally to $\sqrt{I_0 - I}$:[12] a 3D spot starts being formed. This transition is shown in Fig. 1(a) by the arrows.

Let us now consider abrupt transitions. The initial and final states may be of the same or different symmetries, e.g., transitions from a 2D spotless state to states with a well developed 3D spot or a well developed 2D ring spot are both included in the consideration. Let us designate by I_0 the value of I at which the transition occurs. Since such transitions are accompanied by jumps in the discharge parameters, the measured CVC $U(I)$ is discontinuous at $I = I_0$.

There are two possible reasons for abrupt transitions. One of them is the loss of stability of the mode that existed before a transition. Normally, the stability is lost against perturbations that have a symmetry lower than that of the initially existing mode. The other is a fold bifurcation.

Let us consider the first reason. If an abrupt transition occurs in a monotonic way (i.e., without temporal oscillations of the electrode luminosity and discharge parameters, in particular, discharge voltage), then the increment of the perturbations, against which the stability is lost, is real and vanishes at $I = I_0$. Hence, two steady-state solutions exist in the vicinity of the state $I = I_0$: a solution describing the initially existing mode and a solution of a lower symmetry, describing the mode with the perturbations. Hence, a pitchfork bifurcation occurs at $I = I_0$. In order to illustrate this scenario, let us return to the above example and consider the case where the 3D spot-mode solution branches off into the range $I > I_0$, where the 2D spotless-mode solution is stable as shown in Fig. 1(b), a subcritical bifurcation. In this case, the 3D solution is usually unstable in the vicinity of the state $I = I_0$, e.g., Appendix of Ref. 4. If the discharge operates in the spotless mode in the experiment and I is reduced down to values below I_0, the discharge will abruptly switch to another mode, as depicted by the arrows in Fig. 1(b), and this switching will occur in a monotonic way, i.e., without temporal oscillations.

Let us now consider the case where an abrupt transition is accompanied by temporal oscillations. The increment of

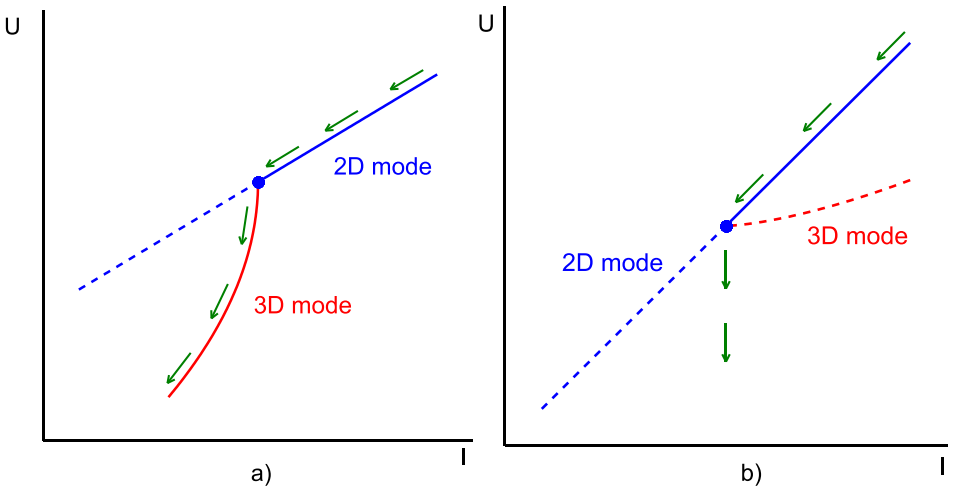

FIG. 1. Schematic of supercritical (a) and subcritical (b) pitchfork bifurcations. Circles: bifurcation points. Dashed line: unstable sections. Solid line: stable sections. Arrows: evolution of regime of current transfer as the discharge current is being reduced.

the perturbations against which the stability is lost is imaginary at $I = I_0$ in this case. Hence, no steady-state solution bifurcates from the initially existing mode at the state $I = I_0$, i.e., the transition is unrelated to a bifurcation of steady-state solutions.

The other possible reason for abrupt transitions is that the mode that existed before the transition has a turning point at $I = I_0$. In other words, this mode has two distinct branches, which exist in the range $I \leq I_0$ (or $I \geq I_0$) and merge at $I = I_0$, so the mode does not exist for $I > I_0$ (or, respectively, $I < I_0$). One can say that the mode has reached the limit of its existence region at $I = I_0$ and turned back, a fold, or saddle-node, bifurcation. If the discharge operates on one of the branches of this mode and the current is increased (or, respectively, decreased), the discharge will abruptly switch to another mode as the value $I = I_0$ has been reached. Given that the increment of the relevant instability vanishes at $I = I_0$,[4] one can expect that the switching occurs in a monotonic way.

In summary, quasi-stationary transitions between states with different symmetries are related to symmetry-breaking (pitchfork) bifurcations of steady-state solutions; abrupt transitions are related to bifurcations of steady-state solutions provided that they occur in a monotonic way, i.e., without temporal oscillations, and the relevant bifurcations are pitchfork or fold.

Discharge vessels are axially symmetric in many experiments. Pitchfork bifurcations of only two types may occur in such configurations.[4,5] First, there is the breaking of axial symmetry, i.e., branching of a 3D mode, where the distribution of luminosity over the electrode surface is periodic in the azimuthal angle with an arbitrary period (2π, or π, or $2\pi/3$, or $\pi/2$, etc.), from a 2D mode, where the distribution of luminosity is axially symmetric. Second, there is the doubling of period with respect to the azimuthal angle, i.e., branching from a 3D mode with one of the periods π, $\pi/2$, $\pi/3$, $\pi/4$, etc., of a 3D mode with double this period. It follows, in particular, that transitions with changes of symmetry of other types cannot occur through pitchfork bifurcations of steady-state solutions, and are always abrupt.

The above general reasoning is valid for mode changes on cathodes and anodes of any DC discharges. This reasoning will be applied to the cases of cathodes of arc and DC glow discharges in Secs. III and IV, respectively.

III. MODE TRANSITIONS ON CATHODES OF ARC DISCHARGES

In the case of refractory cathodes of high-pressure arc discharges, the theory based on the concept of multiple solutions has gone through a detailed experimental validation by means of different methods, such as spectroscopic measurements, electrostatic probe measurements, electrical and pyrometric measurements, and calorimetry; see, e.g., Refs. 13–16 and review 17, and references therein, and also the recent review 18.

The theory of current transfer to cathodes of arc discharges is simpler from the theoretical point of view than the theory for the case of glow discharge. The eigenvalue problem governing the stability of steady-state solutions against small perturbations is self-adjoint (Hermitian) in this case.[19] This means, in particular, that the spectrum of perturbations is real, a conclusion that was confirmed by numerical calculations.[20,21] It follows that all abrupt transitions are monotonic in time. Indeed, no oscillations of arc voltage and luminosity of the cathode surface are observed in the experiments on transitions between diffuse and spot modes on arc cathodes, e.g., Refs. 15, and 22–24. Hence, all abrupt transitions are related to bifurcations of steady-state solutions. In more general terms, any transition between different modes, be it quasi-stationary or abrupt, is related to bifurcations of steady-state solutions in the case of arc cathodes.

In the simplest case of a rod cathode with a flat tip, a 2D diffuse mode of current transfer occurs in the experiment at high currents and a 3D mode with a spot at the edge of the cathode occurs at low currents, as schematically shown by solid lines in Fig. 2. (Note that patterns with several spots have been observed on cathodes of high-pressure arc discharges in more complex arrangements, such as magnetically rotating arcs.[25]) The transitions between the two modes are shown by the arrows in Fig. 2; they are abrupt without temporal oscillations and manifest hysteresis. In agreement with the reasoning of Sec. II, these transitions represent an indication of the presence of pitchfork or fold bifurcations of steady-state solutions.

The latter conclusion may be compared with theoretical results.[19,20] The theory predicts that the diffuse mode and the 3D mode with a spot at the edge of the cathode are the only modes that contain stable sections. The stable and unstable sections of each mode are schematically shown in Fig. 2. In the case of the diffuse mode, these sections are separated by the state B, where a subcritical pitchfork bifurcation occurs. In the case of the spot mode, the stable and unstable sections

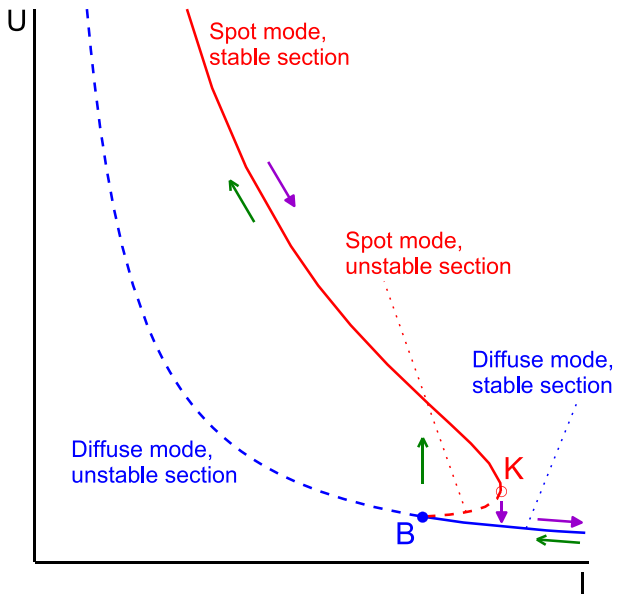

FIG. 2. Schematic of current-voltage characteristics (CVCs) of the diffuse mode of current transfer to rod cathodes of high-pressure arc discharges and of the mode with a spot at the edge of the cathode. The sections shown by the solid lines and the transitions shown by the arrows are observed in the experiment.

are separated by the turning point K, where a fold bifurcation occurs. Thus, the accurate theory indicates that the transition from the diffuse mode to the spot mode is related to the pitchfork bifurcation and the return transition is related to the fold bifurcation, in agreement with the numerical calculations[20,21] and the reasoning of Sec. II. In our view, this provides convincing support to the theory of Sec. II for the case of arc cathodes and no additional modelling is needed.

IV. MODE TRANSITIONS ON CATHODES OF DC GLOW DISCHARGES

A. State-of-the-art of the theory

In the case of DC glow discharges, multiple solutions have been shown to exist even in the most basic models and the solutions computed until now describe many features of the patterns observed, e.g., Ref. 5 and references therein and Ref. 26. In particular, the modelling has shown that self-organization on cathodes of glow microdischarges can occur not only in xenon, but also in other plasma-producing gases, a prediction which has been confirmed by subsequent observations of microdischarges in krypton[27] and argon.[28] On the other hand, the comparison between the theory and the experiment has been merely qualitative until now.

The eigenvalue problem governing the stability of steady-state solutions against small perturbations is not self-adjoint for glow cathodes. Therefore, the spectrum of perturbations need not be real. Indeed, a numerical investigation of stability of 2D modes[29] has given a spectrum that contains both real and complex eigenvalues (and is considerably more elaborate than the spectrum in the case of arc cathodes). It follows that abrupt transitions between different spot patterns may be oscillatory, in contrast to the case of arc cathodes. Note that this conclusion is consistent with the experiment: for example, temporal oscillations of the discharge voltage have been observed in the course of transition from the Townsend to normal discharge.[30–32] Such transitions are unrelated to bifurcations of steady-state solutions.

B. Analyzing experimental observations

A wealth of self-organized spot patterns and transitions between different patterns has been observed on cathodes of DC glow microdischarges.[1,2,27,28,33–41] It follows from Sec. II that a detailed experimental investigation of transitions between different spot patterns, performed with sufficiently small steps in I and a sufficiently high temporal resolution, is needed to unambiguously identify transitions that are related to bifurcations of steady-state solutions. Unfortunately, such investigations seem to be absent. The most detailed data are published in Ref. 40, where the discharge current was adjusted on the microampere scale. The question as to whether the observed transitions are quasi-stationary or abrupt with or without oscillations was not considered. However, transitions between states of different symmetries that seem to be continuous (i.e., quasi-stationary) have been observed, e.g., transitions between states with a large spot occupying the central part of the cathode and a ring-like arrangement of four spots (Ref. 40, Fig. 2), or between a ring spot and a ring-like arrangement of five spots (Ref. 40, Fig. 5). Question arises as to if these transitions can occur through pitchfork bifurcations of steady-state solutions, according to the first scenario described in Sec. II.

In more general terms, one can try to identify in the observations[1,2,27,33–41] all changes of symmetry that may occur through pitchfork bifurcations of steady-state solutions. There is a possibility that these transitions can be realized in a quasi-stationary way, although this is not always the case as exemplified by the transition depicted by the vertical arrow above state B in Fig. 2. On the contrary, transitions that are unrelated to pitchfork bifurcations of steady-state solutions surely cannot be realized in a quasi-stationary way, i.e., are always abrupt.

The discharge vessels are axially symmetric in most of the above-cited experiments. As discussed in the end of Sec. II, pitchfork bifurcations of only two types may occur in such configurations: breaking of axial symmetry and doubling of period with respect to the azimuthal angle. Hence, one should try to identify transitions with changes of symmetry of these two types in the available experimental data.[1,2,27,33–41] If such transitions exist, one should try to find the relevant bifurcations by means of numerical modelling. If the bifurcations have been found, one will be able to compare the computed patterns in the vicinity of the bifurcation points with the patterns observed in the experiments.

Most of the transitions reported in Refs. 1, 2, 27, and 33–41 do not belong to either of the two above types. None of these transitions can occur through bifurcations of steady-state solutions; hence, these transitions cannot be realized in a quasi-stationary way. In particular, this applies to the successive transitions from a ring arrangement with 4 spots to arrangements with 5 and then 6 spots and then back to 5, 4, and 3 spots, which occur as the discharge current is gradually reduced, e.g., Ref. 40, Fig. 2 and Ref. 1, Fig. 2. It is interesting to point out that this conclusion is consistent with the experimental observation that the transition between the ring arrangements of 6, 5, and 4 spots was irreversible: it could be realized when the current is lowered, but attempts to increase the current, when the discharge was operating in these modes, led to the extinction of the discharge.[1]

However, transitions that do belong to one of the two possible types of pitchfork bifurcation (with either a breaking of axial symmetry, or a doubling of period with respect to the azimuthal angle) have been observed and are listed in Table I. Note that the two aforementioned transitions observed in Ref. 40 that appear to be quasi-stationary [those between states with a large spot occupying the central part of the cathode and a ring-like arrangement of four spots (Ref. 40, Fig. 2) and between a ring spot and a ring-like arrangement of five spots (Ref. 40, Fig. 5)] exhibit a breaking of axial symmetry and therefore can indeed occur through pitchfork bifurcations; accordingly, these transitions are listed in the table.

The bifurcation that can be responsible for the second transition in Table I was encountered in Ref. 26. The period-doubling bifurcation that can be responsible for the fifth transition has been encountered as well, although for plasma-producing gases different from xenon, which was used in the experiments:[42] helium (Ref. 43, Fig. 9) and

TABLE I. Transitions between modes with different spot patterns observed on cathodes of glow microdischarges that are potentially related to bifurcations. Numbers in the columns "Symmetry" in cases of 3D modes designate the azimuthal period.

Higher-symmetry mode		Lower-symmetry mode		
Symmetry	Pattern	Symmetry	Pattern	Source
2D	Central spot	3D, π	2 symmetric spots	Reference 1, Figs. 5(c) and 5(d)
2D	Central spot	3D, $\pi/2$	Ring of 4 spots	Reference 1, Fig. 2 and Ref. 40, Fig. 2
2D	Ring spot	3D, $2\pi/5$	Ring of 5 spots	Reference 40, Fig. 5
2D	Central spot, ring spot	3D, $2\pi/5$	Central spot, ring of 5 spots	Reference 40, Fig. 6
3D, $\pi/3$	Ring of 6 spots	3D, $2\pi/3$	2 rings of 3 spots each	Reference 42

krypton (Ref. 27, Fig. 2). In this work, these bifurcations are numerically investigated in detail and the computed patterns in the vicinity of the bifurcation points are compared with the experiment. Also reported in this work is the finding and analysis of the bifurcation that corresponds to the third transition in Table I, for which experimental images taken with a very fine step over discharge current are available (Ref. 40, Fig. 5).

C. Numerical modelling

1. The models

Two numerical models of glow discharges are used in this work, one of them being basic and the other one more detailed. Both models follow standard lines. For completeness, a summary of differential equations, boundary conditions, and data used for transport and kinetic coefficients is given in the Appendix. In brief, the models may be described as follows.

The detailed model comprises equations of conservation of electrons, singly charged atomic ions, singly charged molecular ions, excimers, and an effective species for excited atoms that combines all of the excited states of the 6*s* manifold ($6s[3/2]_2$, $6s[3/2]_1$, $6s'[1/2]_0$, and $6s'[1/2]_1$), Poisson's equation, and an equation for the conservation of electron energy. Transport equations for charged-particle species and electron energy density are written in the drift-diffusion approximation, and transport equations for the excited neutral species describe diffusion. The geometry considered is that of the so-called cathode boundary layer discharge device (Fig. 3). This geometry was used in the vast majority of the experiments[1,2,27,33–41] and comprises a flat cathode and a perforated anode, separated by a dielectric, with the radius of the opening in the anode equal to the radius of the discharge cavity in the dielectric. It is assumed that the charged and excited particles coming from the plasma are absorbed, and subsequently neutralized and deexcited, respectively, at the surfaces of the electrodes and the dielectric.

The above-described detailed model is computationally costly and therefore not suitable for the serial 3D simulations required for the purposes of this work. It was shown previously experimentally[36] and computationally[26] that self-organized patterns in the cathode boundary layer discharge and a discharge with a parallel-plane electrode configuration are qualitatively similar. An account of detailed chemical kinetics does not produce a qualitative effect as well.[43] Therefore, most of the simulations reported below have been performed by means of a more basic model, which relies on a simple chemical kinetic scheme and assumes a parallel-plane electrode configuration. (We note that the spot patterns computed in the framework of the basic and detailed models turned out to be qualitatively similar, in agreement with the above.) The basic model takes into account only one ion species (molecular ions) and the only ionization channel (direct ionization from the ground state by electron impact) with a rapid conversion of the produced atomic ions into molecular ions, and employs the local-field approximation (i.e., the electron kinetic and transport coefficients are treated as known functions of the local reduced electric field). The discharge vessel is assumed to be a cylinder with the end faces being the electrodes and the lateral surface being insulating. The neutralization of the ions and the electrons at the dielectric is neglected, so particles coming from the plasma are reflected back. Note that the effect of the neutralization has been well understood by now (e.g., Ref. 26 and references therein); as far as 3D spots are concerned, it results in the migration of spots away from the wall in the direction to the center of the cathode.[43] With this in mind, the assumption of negligible neutralization is sufficient for

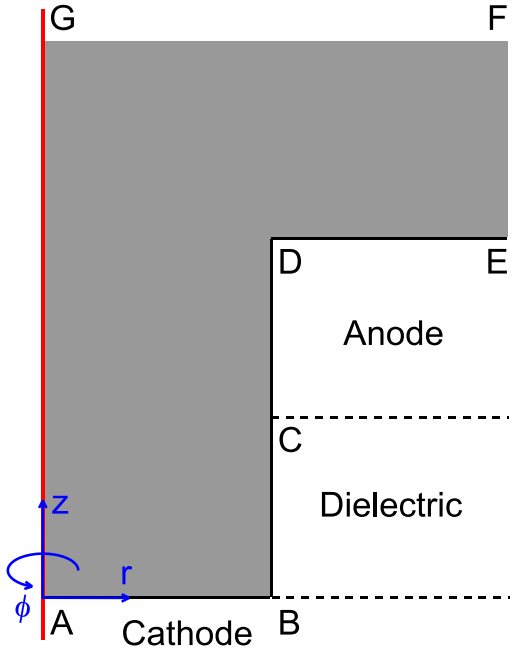

FIG. 3. Schematic of the cathode boundary layer discharge vessel. *AG* is the axis of symmetry.

most purposes of this work, while making computations less costly and easier to analyze.

2. Identifying the relevant bifurcations

Results of simulations reported in this section have been obtained by means of the basic model for the following conditions: a discharge in xenon under the pressure of 30 Torr, the electron temperature $T_e = 1$eV, the heavy-particle temperature $T_h = 300$K, the interelectrode gap and discharge radius both of 0.5mm, and the secondary electron emission coefficient $\gamma = 0.03$.

In order to show the place of the bifurcations being investigated (those corresponding to the second, third, and fifth transitions in Table I) in the general pattern of self-organization in DC glow microdischarges, we will briefly introduce the latter, referring to Ref. 5 for details. In the framework of the basic model, the problem admits a 1D solution describing a mode in which all the variables depend only on the axial variable. This mode exists at all values of the discharge current and may be termed the fundamental mode. There are also multidimensional modes which bifurcate from, and rejoin, the fundamental mode, the so-called second-generation modes. Figure 4 depicts the current-voltage characteristics (CVCs) of the fundamental mode and the first five second-generation modes. In Fig. 4, $\langle j \rangle$ is the average current density evaluated over a cross section of the discharge vessel (which is proportional to the discharge current). The schematics illustrate distributions of current density on the cathode surface associated with each mode. a_i and b_i designate bifurcation points where second-generation modes branch off from and rejoin the fundamental mode. The modes are ordered by decreasing separation of the related bifurcation points: the mode designated a_1b_1 is the one with the bifurcation points a_1 and b_1 positioned farthest apart, the mode a_2b_2 is the one with the second largest separation between the bifurcation points, and so on.

The modes a_1b_1 and a_3b_3 have been computed previously (Refs. 44 and 45, respectively) and are included in Fig. 4 for the sake of completeness; we only note that a_1b_1 is 3D with the azimuthal period of 2π, while a_3b_3 is 2D with one branch associated with a spot at the center of the cathode and the other branch with a ring spot at the periphery of the cathode. The other modes, a_2b_2, a_4b_4, and a_5b_5, are 3D with periods π, $2\pi/3$, and $\pi/2$, respectively. The evolution with discharge current of the cathodic spot patterns associated with these modes is shown in Fig. 5. Let us consider first the evolution of the patterns associated with the mode a_2b_2 [Fig. 4(a)]. The state 151.05 V is positioned in the vicinity of the bifurcation point a_2, and the spot pattern comprises two very diffuse cold spots at the periphery of the cathode. Further away from a_2, the cold spots expand and at state 151.79 V start merging. This corresponds to the retrograde section of the CVC a_2b_2 seen in Fig. 4(b) in a narrow current range around 280Am^{-2}. As current is further reduced towards b_2, the two cold spots expand further and the resulting pattern comprises two well-pronounced hot spots at the periphery, state 160.4 V. Note that this pattern is similar to those observed in the experiment; cf. Ref. 1, Fig. 5. Finally, the state 173.93 V is

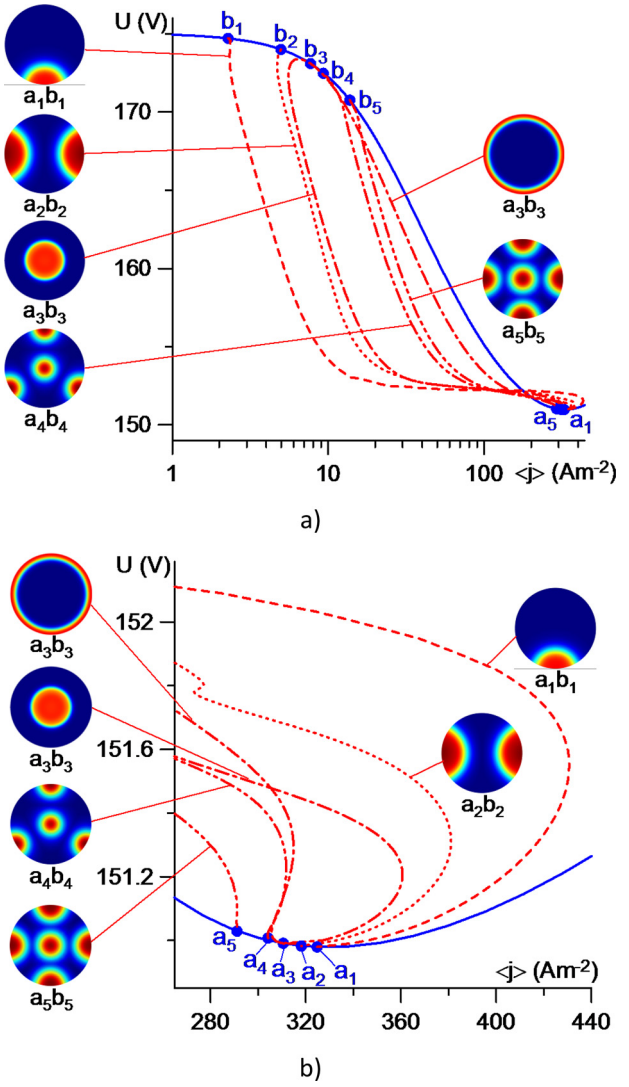

FIG. 4. CVCs. Solid: the 1D (fundamental) mode. Dashed-dotted: 2D mode a_3b_3. Other lines: different 3D modes. Circles: bifurcation points. (a) General view. (b) Details near the point of minimum of the CVC of the 1D mode.

positioned in the vicinity of the bifurcation point b_2 and the hot spots are very diffuse.

The patterns associated with the mode a_4b_4 are shown in Fig. 5(b). The state 151.01 V is positioned in the vicinity of the bifurcation point a_4 and the pattern comprises three very diffuse cold spots at the periphery. Further away from a_4, the spots become better pronounced and a cold spot appears at the center, states 151.15 V and 151.53 V. Note that similar patterns with three hot spots have been observed in the experiment, cf. Ref. 1, Fig. 5 and Ref. 40, Fig. 2. As current is further reduced towards b_4, the cold spot at the center is gradually transformed into a hot spot. The hot spots become well pronounced and a pattern comprising three (hot) spots at the periphery and a central spot is formed, state 151.74 V (the pattern is shown in the schematic in Fig. 4). Note that patterns with three spots at the periphery and a spot at the center similar to that of the state 151.74 V have also been observed in the experiment, cf. Ref. 38, Fig. 4. Note also that the transition between patterns with well-defined cold and hot spots is not accompanied by retrograde behavior, in

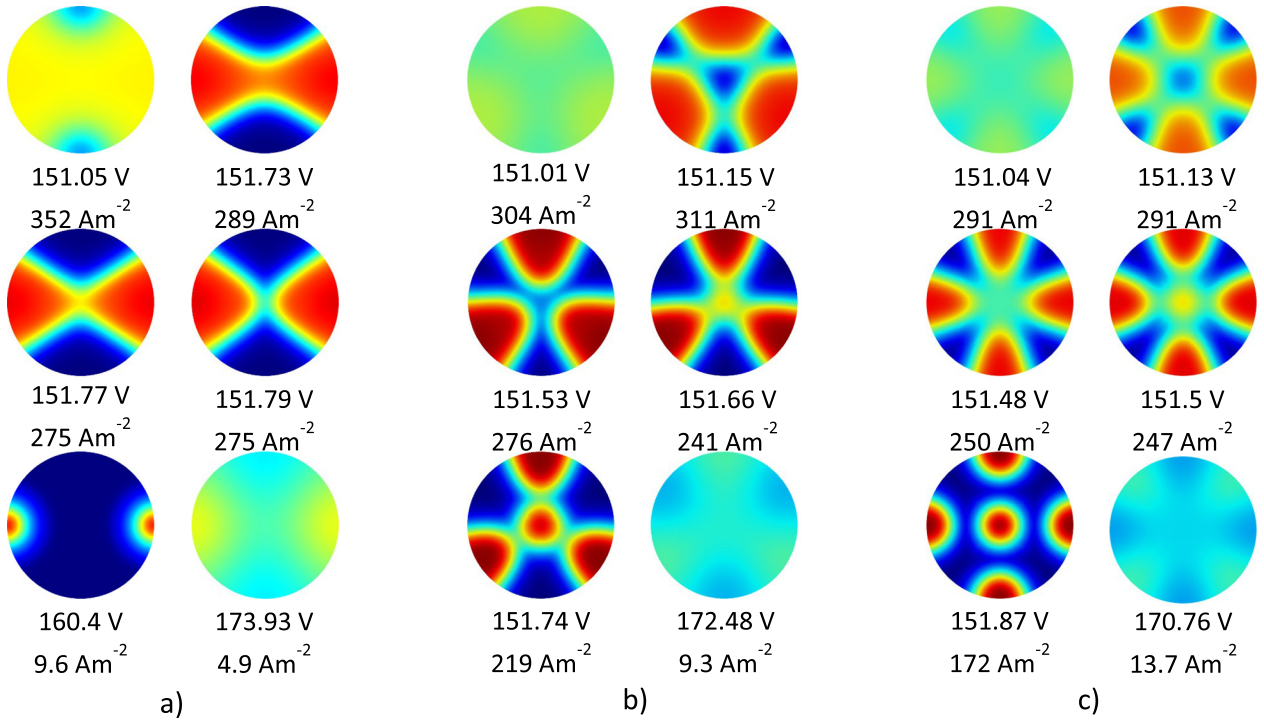

FIG. 5. Evolution of distributions of current on the surface of the cathode associated with different modes. (a) Mode a_2b_2. (b) a_4b_4. (c) a_5b_5.

contrast with the case of the mode a_2b_2. The state 172.48 V is positioned in the vicinity of the bifurcation point b_4 and the hot spots are very diffuse.

The evolution of patterns associated with the mode a_5b_5 shown in Fig. 5(c) follows the same trend as the mode a_4b_4. Note that patterns with four spots at the periphery have also been observed in the experiment, cf. Ref. 1, Fig. 2 and Ref. 40, Fig. 2.

A convenient graphical representation, or bifurcation diagram, of the modes a_4b_4 and a_5b_5 is given in Fig. 6 with the use of the coordinates $(\langle j\rangle, j_c)$, where j_c is the current density at the center of the cathode. This representation allows a quick identification of the state where the switching between patterns comprising cold and hot spots at the center happens: it is the point in Fig. 6 where the line representing the mode in question intersects the straight line representing the 1D mode. For currents higher than the one corresponding to the switching, the current density at the center is lower than that corresponding to the 1D mode and the pattern comprises a cold spot at the center; $j_c > \langle j\rangle$ for lower currents and the pattern comprises a hot spot at the center.

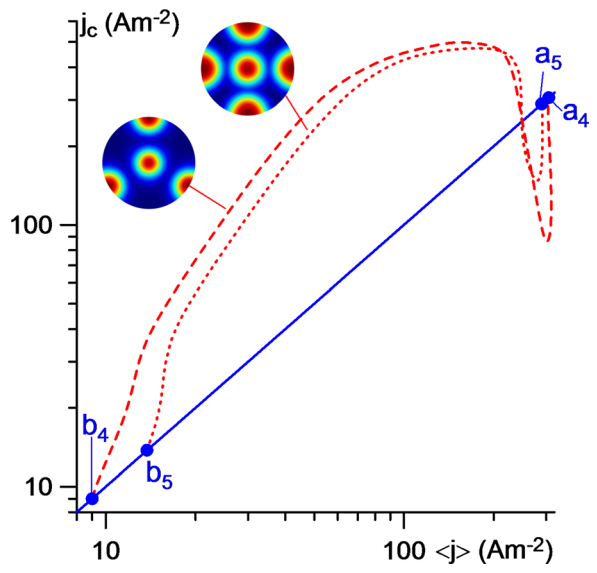

FIG. 6. Bifurcation diagram. Solid: the 1D (fundamental) mode. Dashed, dotted: 3D second-generation modes a_4b_4 and a_5b_5. Circles: bifurcation points.

Breaking of axial symmetry occurring at the state a_5 (Figs. 4 and 6) corresponds to the second transition in Table I. In order to identify bifurcations corresponding to the third and fifth transitions, one needs to consider third-generation modes, i.e., 3D modes that branch off from and rejoin second-generation modes.

Three third-generation modes bifurcating from the mode a_3b_3, designated $a_{3,1}b_{3,1}$, $a_{3,2}b_{3,2}$, and $a_{3,3}b_{3,3}$, are shown in Fig. 7. They branch off from and rejoin that branch of the mode a_3b_3 which is associated with a ring spot at the periphery; the bifurcations are breaking of axial symmetry. The modes $a_{3,1}b_{3,1}$, $a_{3,2}b_{3,2}$, and $a_{3,3}b_{3,3}$ have the periods of $2\pi/3$, $2\pi/5$, and $\pi/3$, respectively, and are associated with spot patterns comprising three spots at the periphery of the cathode, five spots, and six spots, respectively. Since none of the patterns shown in Fig. 7 comprise a spot at the center, the coordinates $(\langle j\rangle, j_c)$ would be inconvenient and the coordinates $(\langle j\rangle, j_e)$ are used, where j_e is the current density at a fixed point on the periphery of the cathode which coincides with the center of one of the spots.

The evolution of the spot patterns associated with the mode $a_{3,2}b_{3,2}$ is shown in Fig. 8. At state 151.82 V, which is positioned near the bifurcation point $a_{3,2}$, the ring spot is slightly non-uniform in the azimuthal direction. Further

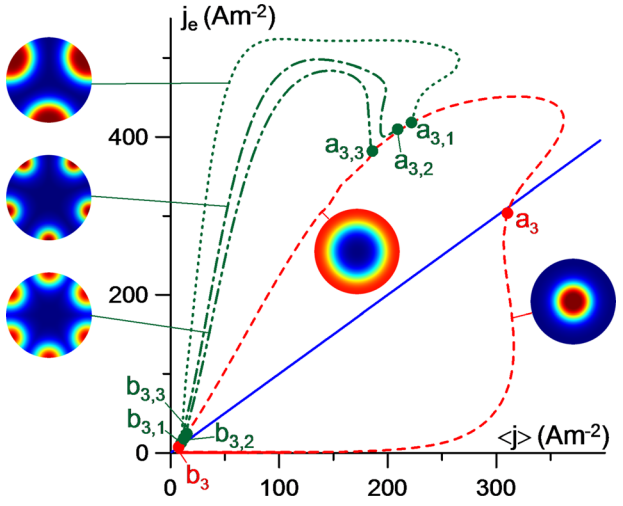

FIG. 7. Bifurcation diagram. Solid: the 1D (fundamental) mode. Dashed: 2D mode a_3b_3. Other lines: 3D modes. Circles: bifurcation points.

away from $a_{3,2}$, the non-uniformity evolves into well-pronounced spots (states 151.81 V and 151.84 V). The spots become smaller as the current is further reduced (state 152.26 V). As the bifurcation point $b_{3,2}$ is approached, the spots expand once again (state 167.94 V). In the close vicinity of $b_{3,2}$ (state 170.70 V), a ring spot with a weak non-uniformity in the azimuthal direction is seen. Note that patterns similar to those shown in Fig. 8 have been observed in the experiment (Ref. 40, Fig. 5).

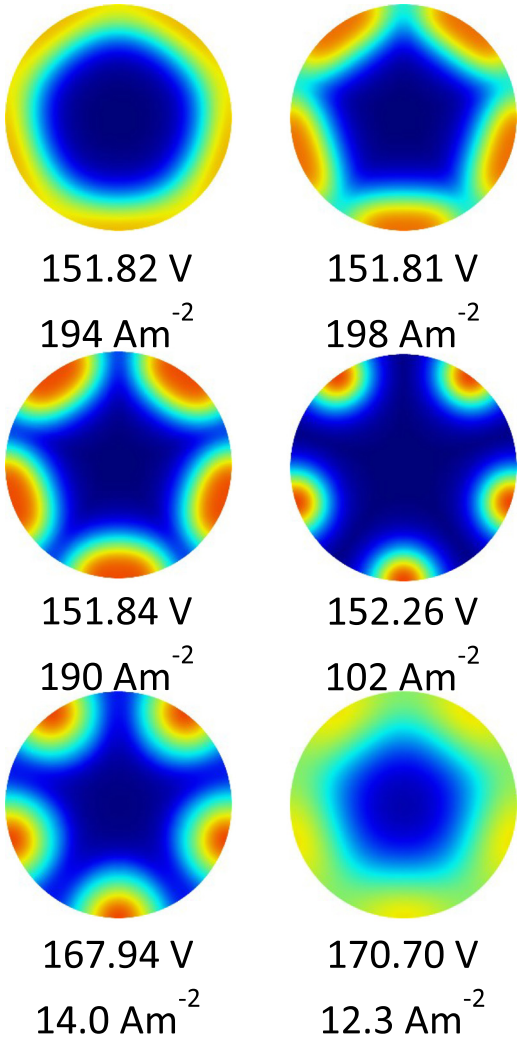

FIG. 8. Evolution of distribution of current on the surface of the cathode associated with the mode $a_{3,2}b_{3,2}$.

The behavior of the modes $a_{3,1}b_{3,1}$ and $a_{3,3}b_{3,3}$ follows the same trend as the behavior of the mode $a_{3,2}b_{3,2}$. The patterns are similar to experimentally observed patterns comprising three and six spots inside the cathode; cf. Ref. 1, Figs. 2 and 5 and Ref. 40, Fig. 2. Note, however, that the pattern with three spots associated with the mode $a_{3,1}b_{3,1}$ is similar to the pattern with three spots appearing in some states belonging to a_4b_4 [states 151.15 V and 151.53 V in Fig. 5(b)] and it is difficult to know which one of these two modes was observed in the experiments.[1,40] A similar comment applies to the mode $a_{3,3}b_{3,3}$.

Breaking of axial symmetry occurring at the states $a_{3,2}$ and $b_{3,2}$ in Fig. 7 corresponds to the third transition in Table I. The bifurcation corresponding to the fifth transition is period doubling occurring at the state $a_{10,1}$ in Fig. 9. Here, $a_{10}b_{10}$ is a second-generation mode with the period of $\pi/3$ and $a_{10,1}b_{10,1}$ is a third-generation mode with the period of $2\pi/3$. The period doubling at $a_{10,1}$ occurs as follows: every second spot gradually moves from the periphery towards the center of the cathode; eventually a central spot is formed. (Note that the image illustrating the mode $a_{10,1}b_{10,1}$ in Fig. 9 corresponds to the situation where the central spot has already been formed.) This is similar to how the similar bifurcation occurs in helium (Ref. 43, Fig. 9) and krypton (Ref. 27, Fig. 2) except that in krypton the central spot is already present at the bifurcation point $a_{10,1}$.

D. Comparing the modelling and the experiment

As discussed in Sec. IV C 2, the bifurcation corresponding to the second transition in Table I is breaking of axial

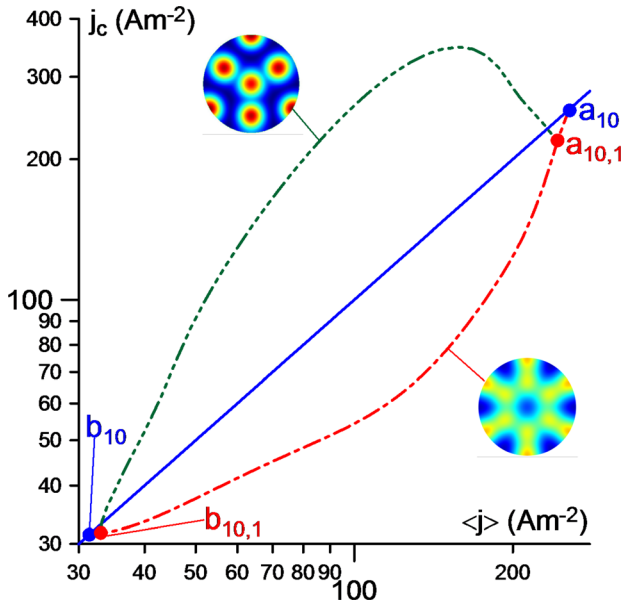

FIG. 9. Bifurcation diagram. Solid: the 1D (fundamental) mode. Dashed: 3D second-generation mode $a_{10}b_{10}$. Dotted: 3D third-generation mode $a_{10,1}b_{10,1}$. Circles: bifurcation points.

symmetry occurring at the state a_5 (Figs. 4 and 6), where a mode with a ring-like arrangement of four spots (mode a_5b_5) branches off from the (fundamental) mode with an axially symmetric spot occupying the whole cathode surface except for the periphery (the abnormal discharge). The bifurcation corresponding to the third transition is breaking of axial symmetry occurring at the states $a_{3,2}$ and $b_{3,2}$ (Fig. 7), where a mode with a ring-like arrangement of five spots (mode $a_{3,2}b_{3,2}$) branches off from the axially symmetric mode with a ring spot (a_3b_3). The bifurcation corresponding to the fifth transition is period doubling occurring at the state $a_{10,1}$ (Fig. 9), where the mode $a_{10,1}b_{10,1}$, which is associated with three spots at the periphery and three spots closer to the center and has the period of $2\pi/3$, branches off from the mode $a_{10}b_{10}$, which is associated with a ring-like arrangement of 6 identical spots at the periphery and has the period of $\pi/3$.

The computed patterns in the vicinity of the bifurcation points are compared with the patterns observed in the experiments in Fig. 10. The experimental images shown in Figs. 10(a) and 10(b) have been taken from Figs. 2 and 5, respectively, of Ref. 40. Those shown in Fig. 10(c) have been kindly provided by Zhu and Niraula;[42] we note for completeness that the geometry in this experiment was the same as in Ref. 40, the Xe pressure was 100 Torr, and the current and voltage were nearly the same for both frames: 0.155 mA and 278 V.

The first one of the computed images shown in Fig. 10(a) represents the bifurcation point a_5. The other images correspond to states belonging to the mode a_5b_5 in the vicinity of a_5. The last one of the computed images shown in Fig. 10(b) represents the bifurcation point $a_{3,2}$, the other images correspond to states belonging to the mode $a_{3,2}b_{3,2}$ in the vicinity of $a_{3,2}$. The first one of the computed images shown in Fig. 10(c) represents the bifurcation point $a_{10,1}$, the other images correspond to states belonging to the mode $a_{10,1}b_{10,1}$ in the vicinity of $a_{10,1}$.

It is seen from Fig. 10 that the computed patterns in the vicinity of the bifurcation points closely resemble the patterns observed in the experiments. This supports the hypothesis that the transitions between patterns of different symmetries observed in the experiment and listed in the second, third, and fifth lines of Table I are quasi-stationary and occur through pitchfork bifurcations.

The transition between the abnormal discharge and a mode with four spots, shown in Fig. 10(a), resembles the well-known transition between the abnormal and normal glow discharges, the difference being that there are four spots in the 3D mode and not just one as in the normal discharge. A question arises as to what is the reason for this difference and why just four spots are formed and not two or three. This question is related to a more general question as to why patterns with multiple spots have been observed in glow microdischarges but not in regular-scale glows and is of significant interest.

It is seen from Fig. 4 that the modes with one, two, and three spots branch off, at the states a_1, a_2, and a_4, through subcritical bifurcations. On the other hand, the mode with four spots at the periphery branches off from the mode with an axially symmetric spot occupying the whole cathode surface except for the periphery (the abnormal discharge), at the state a_5, through a bifurcation which is supercritical, albeit marginally. (Note that this is a typical situation: low- and high-order second-generation modes tend to branch off through, respectively, subcritical and supercritical bifurcations Ref. 5, Fig. 3.) As discussed in Sec. II, a usual necessary condition for a quasi-stationary transition between two steady-state modes connected by a pitchfork bifurcation is that the bifurcation be supercritical. Therefore, it may seem that the modelling results shown in Fig. 4 explain why the abnormal discharge in the experiment with microdischarges goes into the mode with four (rather than one, two, or three) spots, as seen in Fig. 10(a). On the other hand, the experimental CVC of this transition [(Ref. 40, Fig. 3(a)] apparently represents a diagram of a subcritical bifurcation, and so does also the CVC shown in Ref. 1, Fig. 3(a). Thus, there is a discrepancy between the measurements, on the one hand, and numerical modelling and the usual trend of the bifurcation theory, on the other. The other discrepancy between the measured and computed CVCs is that the discharge voltage in the 3D mode is lower than that in the (axially symmetric) abnormal mode in the experiment but higher in the modelling.

One could think that the discrepancies are due to simplifications, employed in the (basic) model used in the above modelling. In order to clarify this point, the bifurcations occurring at the states a_4 and a_5 have been recomputed by means of the detailed model, described in Sec. IV C 1 and Appendix. The results are shown in Fig. 11. Since the geometry of the discharge vessel and the boundary conditions describing absorption of the charged particles at the wall invalidate the 1D solution, the role of the fundamental mode (abnormal discharge) is played by the first 2D mode.[5] All second-generation solutions are 3D, and the first four modes, which have the periods of 2π, π, $2\pi/3$, and $\pi/2$, respectively, are designated a_1b_1, a_2b_2, a_4b_4, and a_5b_5 (i.e., the designation a_3b_3 is skipped in order to maintain consistency with the designations of the second-generation modes computed in the framework of the basic model).

It is seen from Fig. 11 that the patterns of the solutions are similar to those computed in the framework of the basic model, in agreement with what was said in Sec. IV C 1. The account of neutralization of the charged particles at the wall of the vessel causes the spots to migrate from the edge to the inside of the cathode, also in agreement with Sec. IV C 1. The discharge voltage computed in the framework of the detailed model is significantly higher than the voltage in the basic model. The bifurcation occurring at a_5 becomes marginally subcritical, while the one at a_4 remains clearly subcritical, as well as those at a_1 and a_2, which are not shown in Fig. 11. The discharge voltage in the 3D modes is slightly higher than that in the fundamental mode. Thus, the above-described discrepancy has not been resolved and further computational and experimental work is needed.

V. SUMMARY AND THE WORK AHEAD

The existence, or not, of bifurcations of steady-state solutions describing different modes of current transfer to electrodes of DC discharges is related to the underlying physics and is therefore of significant interest. Bifurcations manifest

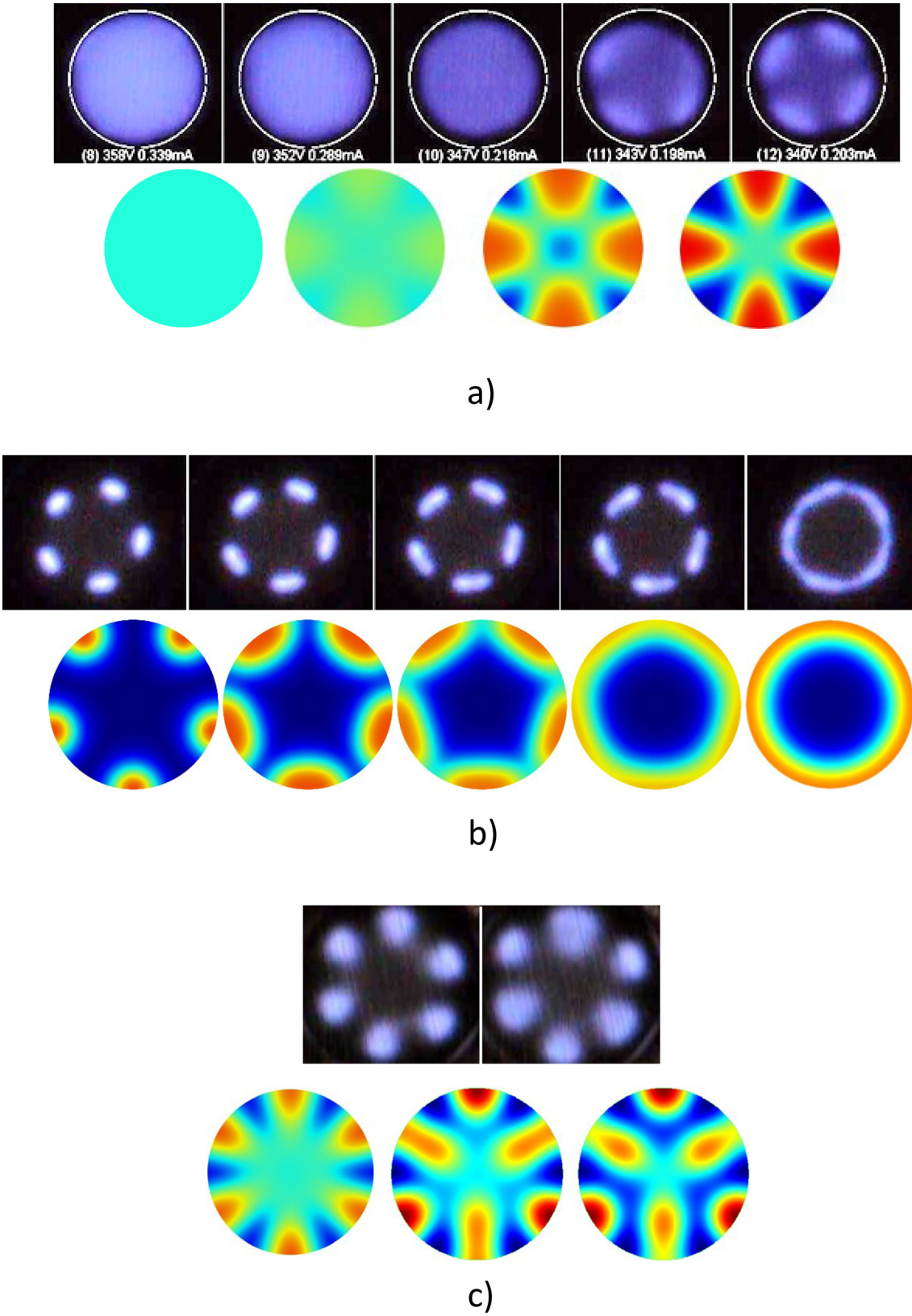

FIG. 10. Experimentally observed and computed transitions between different modes in xenon.

themselves in the experiment as transitions between modes with different spot patterns, which occur as the discharge current I is varied. Two scenarios of such transitions are possible: (1) quasi-stationary (continuous) and, consequently, reversible transitions between states where distributions of luminosity over the electrode surface possess different symmetries and (2) transitions that occur abruptly even for very small variations of I. Quasi-stationary transitions are related to a symmetry-breaking (pitchfork) bifurcation. If the discharge vessel is axially symmetric, pitchfork bifurcations of

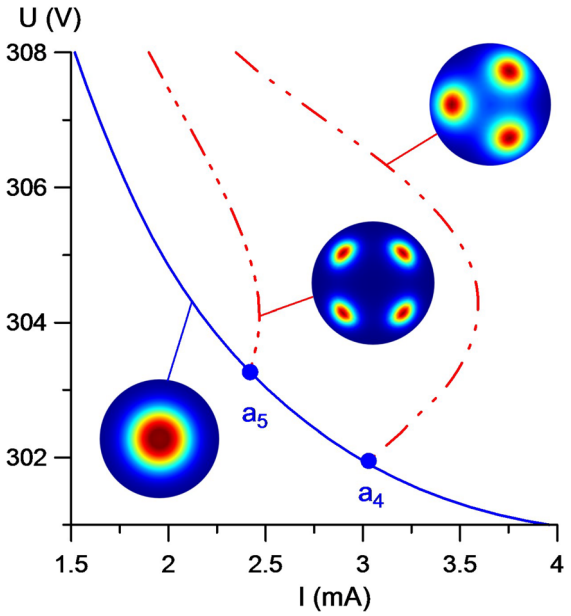

FIG. 11. CVCs, detailed model. Solid: the first 2D (the fundamental) mode. Other lines: 3D modes a_4b_4 and a_5b_5. Circles: bifurcation points.

only two types may occur: breaking of axial symmetry and doubling of period with respect to the azimuthal angle. Abrupt transitions that occur in a monotonic way, i.e., without temporal oscillations, are related to pitchfork or fold bifurcations. Finally, abrupt transitions accompanied by temporal oscillations are unrelated to a bifurcation of steady-state solutions.

The above general reasoning is valid for mode changes on cathodes and anodes of any DC discharges. In the case of (refractory) cathodes of high-pressure arc discharges, the eigenvalue problem governing the stability of steady-state solutions against small perturbations is self-adjoint and its spectrum is real. Therefore, all abrupt transitions are monotonic in time, in agreement with what is known from the numerical modelling and the experiment. It follows that any transition between different modes, be it quasi-stationary or abrupt, is related to a bifurcation of steady-state solutions in the case of arc cathodes. Thus, transitions between diffuse and spot modes of current transfer, frequently observed in the experiment, represent an indication of the presence of pitchfork or fold bifurcations of steady-state solutions.

A wealth of spot patterns and transitions between different patterns have been observed on cathodes of DC glow microdischarges.[1,2,27,33–41] In particular, transitions between states of different symmetries that seem to be continuous (i.e., quasi-stationary) have been observed in Ref. 40. It is legitimate to hypothesize that such transitions occur through pitchfork bifurcations (breaking of axial symmetry or period doubling) of steady-state solutions according to the first above-mentioned scenario. This hypothesis has been confirmed by numerical modelling: the relevant bifurcations have been investigated numerically and the computed patterns in the vicinity of the bifurcation points are found to closely resemble the patterns observed in the course of the transitions in the experiment. Note that new 3D modes of current transfer were computed in the course of finding the bifurcations and these new modes are associated with experimental spot patterns reported in the literature.

Thus, available experimental data on multiple modes of current transfer to cathodes of DC glow and arc discharges provide clear indications of the presence of pitchfork or fold bifurcations of steady-state solutions, as predicted by the theory. While the comparison between the theory and the experiment still remains qualitative in the case of DC glow cathodes, the agreement is convincing and lends further support to the theory.

A detailed experimental investigation of transitions between different spot patterns on cathodes of glow microdischarges, performed with sufficiently small steps in I and a sufficiently high temporal resolution and accompanied by numerical modelling, would allow verification of the above scenarios. For example, it would be very interesting to verify the theoretical prediction that successive transitions between ring arrangements of 4, 5, 6, 5, 4, and 3 spots shown in, e.g., Ref. 40, Fig. 2 and Ref. 1, Fig. 2 cannot be realized in a quasi-stationary way, in contrast to the second, third, and fifth transitions in Table I. It should be stressed that this prediction is consistent with the experimental observation that the transition between the ring arrangements of 6, 5, and 4 spots was irreversible.[1] Note also that the theory predicts that any transition, except those between an axially symmetric mode and a 3D mode and those between 3D modes with doubling of azimuthal period, will be abrupt even for very small variations of discharge current and/or voltage.

Another interesting question to be addressed is the one discussed in the end of Sec. IV D and concerns the discrepancy between the measured CVC of the transition from the abnormal discharge and the mode with four spots, on the one hand, and numerical modelling as well as the usual trend of the bifurcation theory, on the other hand.

ACKNOWLEDGMENTS

This work was supported by FCT—Fundação para a Ciência e a Tecnologia of Portugal through the project PEst-OE/UID/FIS/50010/2013. The authors are grateful to Dr. Wei Dong Zhu and Mr. Prajwal Niraula for discussion of the experiment[40] and kindly providing the experimental images shown in Fig. 10(c).

APPENDIX: EQUATIONS AND BOUNDARY CONDITIONS

The system of differential equations describing the detailed model reads

$$\begin{aligned}
&\nabla\cdot\mathbf{J}_e = S_e, \quad \mathbf{J}_e = -D_e\nabla n_e + n_e\mu_e\nabla\varphi;\\
&\nabla\cdot\mathbf{J}_\varepsilon = e\mathbf{J}_e\cdot\nabla\varphi - S_\varepsilon, \quad \mathbf{J}_\varepsilon = -D_\varepsilon\nabla n_\varepsilon + n_\varepsilon\mu_\varepsilon\nabla\varphi;\\
&\nabla\cdot\mathbf{J}_{i\beta} = S_{i\beta}, \quad \mathbf{J}_{i\beta} = -D_{i\beta}\nabla n_{i\beta} - n_{i\beta}\mu_{i\beta}\nabla\varphi;\\
&\nabla\cdot\mathbf{J}_{ex\beta} = S_{ex\beta}, \quad \mathbf{J}_{ex\beta} = -D_{ex\beta}\nabla n_{ex\beta};\\
&\varepsilon_0\nabla^2\varphi = -e\,(n_{i1} + n_{i2} - n_e).
\end{aligned} \tag{A1}$$

Here, $\beta = 1, 2$; the indexes $e, \varepsilon, i1, i2, ex1, ex2$ refer to electrons, electron energy density, atomic ions, molecular ions, atoms in excited states, and excimers, respectively; n_α, $\mathbf{J}_\alpha$, D_α, μ_α, S_α are the number density, density of the transport flux, diffusion coefficient, mobility, and rate of production of particles per unit time and unit volume of species α ($\alpha = e, i1, i2, ex1, ex2$); the electron energy density is defined as $n_\varepsilon = n_e\bar{\varepsilon}$, where $\bar{\varepsilon}$ is the average electron energy, and coincides with 3/2 of the electron pressure; $\mathbf{J}_\varepsilon$ is the density of electron energy flux; D_ε and μ_ε are the so-called electron energy diffusion coefficient and mobility; S_ε is the rate of loss of electron energy per unit time and unit volume due to collisions; φ is electric potential; ε_0 is permittivity of free space, and e is the elementary charge. The transport coefficients used are the same as in Ref. 43. The set of reactions comprises electron impact ionization from the ground state, an effective excited atomic state, and the metastable molecular state; excitation of atoms by electron impact; atomic ion conversion to molecular ions with neutral atoms playing the role of the third body; metastable pooling; dissociative recombination; photon emission from the atomic and molecular excited states; conversion of excited atoms to excimers with neutral atoms playing the role of the third body. The kinetic coefficients are the same as in Ref. 43.

The computation domain corresponds to the cathode boundary layer discharge device; Fig. 3. Let us introduce cylindrical coordinates (r, ϕ, z) with the origin at the center of the cathode and the z-axis coinciding with the axis of the vessel. The boundary conditions for Eq. (A1) are written in the conventional form (e.g., Refs. 46 and 47)

$$
\begin{aligned}
&J_{\alpha z} = \frac{1}{4}\sqrt{\frac{8k_BT_\alpha}{\pi m_\alpha}}n_\alpha, \quad J_{ez} = -\gamma J_{iz} - \gamma J_{i2z},\\
&J_{\varepsilon z} = (E_I - 2W)J_{ez}, \quad \varphi = 0\,; \quad J_{\alpha n} = \frac{1}{4}\sqrt{\frac{8k_BT_\alpha}{\pi m_\alpha}}n_\alpha,\\
&J_{en} = \frac{1}{2}\sqrt{\frac{8k_eT_e}{\pi m_e}}n_e, \quad J_{\varepsilon n} = \frac{1}{2}\sqrt{\frac{8k_BT_e}{\pi m_e}}n_\varepsilon, \quad \varphi = U;\\
&J_{\alpha r} = \frac{1}{4}\sqrt{\frac{8k_BT_\alpha}{\pi m_\alpha}}n_\alpha, \quad J_{er} = \frac{1}{2}\sqrt{\frac{8k_eT_e}{\pi m_e}}n_e,\\
&J_{\varepsilon r} = \frac{1}{2}\sqrt{\frac{8k_BT_e}{\pi m_e}}n_\varepsilon, \quad J_{i1r} + J_{i2r} - J_{er} = 0,
\end{aligned}
\tag{A2}
$$

at the surface of the cathode (line AB in Fig. 3), anode (CDE), and dielectric (BC), respectively. Here, γ is the effective secondary emission coefficient, which is assumed to characterize all mechanisms of electron emission (due to ion, photon, and excited species bombardment);[48] E_I is the ionization energy of the incident ions; W is the work function of the cathode surface; U is the discharge voltage; the subscripts r, z, and n denote radial, axial, and normal projections of the corresponding vectors (the normal n points outwards from the computation domain); $\alpha = i1, i2, ex1, ex2$; k_B is Boltzmann's constant; $T_\alpha = T_h$, where T_h is the heavy-particle temperature (a given parameter); $T_e = 2\bar{\varepsilon}/3k_B$ is the electron temperature; and m_α are the particle masses.

Results of simulations performed by means of this model, reported in this work, refer to the following conditions: discharge in xenon under the pressure of 75 Torr, $T_h = 300$ K, $\gamma = 0.075$, the cavity radius $|AB| = 0.375$ mm, the thickness of the dielectric $|BC| = 0.25$ mm, and the height of the anode $|CD| = 0.25$ mm.

The system of differential equations describing the basic model comprises the first and last equations in Eq. (A1) and the third equation written for only one ion species. Boundary conditions at the cathode, anode, and dielectric are written as, respectively,

$$
\begin{aligned}
&z = 0: \quad \frac{\partial n_i}{\partial z} = 0, \quad J_{ez} = -\gamma J_{iz}, \quad \varphi = 0\,;\\
&z = h: \quad n_i = 0, \quad \frac{\partial n_e}{\partial z} = 0, \quad \varphi = U;\\
&r = R: \quad \frac{\partial n_i}{\partial r} = \frac{\partial n_e}{\partial r} = 0\,, \quad J_{ir} - J_{er} = 0,
\end{aligned}
\tag{A3}
$$

where n_i and $\mathbf{J}_i$ are the number density and transport flux density of the ions. The first boundary condition in the first line and the second boundary condition in the second line imply that diffusion fluxes of the attracted particles at the electrode surfaces are neglected compared to drift. The first and second boundary conditions in the third line imply that the neutralization of the ions and the electrons at the dielectric is neglected. The transport and kinetic coefficients used in the basic model for xenon are taken from Ref. 45.

Numerical results reported in this work have been computed using the commercial finite element software COMSOL Multiphysics. The detailed model was implemented using the Plasma module of COMSOL, which was adapted so that it could be used in combination with a stationary solver and supplemented with a mesh element size based stabilization method to reduce the Péclet number. The basic model was implemented using the Transport of Diluted Species module, and also solved using a stationary solver.

Two procedures have been used in this work to compute multiple modes. One of them is the procedure described in Ref. 5, which can be briefly summarized as follows. First, one computes the fundamental mode in a wide range of current. The stability of the fundamental mode is then tested by the eigenvalue solver, for each value of current, against perturbations that have a lower symmetry than the fundamental mode. A bifurcation point is found where the stability of the fundamental mode is lost to such perturbations. The non-fundamental mode is computed with a stationary solver using a parametric sweep of a control parameter (discharge current or voltage), starting from the vicinity of the bifurcation point.

The other procedure used in this work was as follows. A parametric sweep of a control parameter is performed on the fundamental mode with a stationary solver in the 3D computation domain. (The computation domain is 2D in cases where a 2D non-fundamental mode branching off from the 1D fundamental mode is sought.) The solver computes solutions along the fundamental mode until it passes a bifurcation point, where it can switch to a non-fundamental mode. In this way, one may compute bifurcations and non-fundamental modes without using the eigenvalue solver.

[1]N. Takano and K. H. Schoenbach, Plasma Sources Sci. Technol. **15**, S109 (2006).
[2]W. Zhu, N. Takano, K. H. Schoenbach, D. Guru, J. McLaren, J. Heberlein, R. May, and J. R. Cooper, J. Phys. D: Appl. Phys. **40**, 3896 (2007).
[3]Z. Chen, S. Zhang, I. Levchenko, I. I. Beilis, and M. Keidar, Sci. Rep. **7**, 12163 (2017).
[4]P. G. C. Almeida, M. S. Benilov, M. D. Cunha, and M. J. Faria, J. Phys. D: Appl. Phys. **42**, 194010 (2009).
[5]M. S. Benilov, Plasma Sources Sci. Technol. **23**, 054019 (2014).
[6]M. S. Bieniek, P. G. C. Almeida, and M. S. Benilov, in *Proceedings of the XXXIII ICPIG*, Estoril, Portugal, 9–14 July (2017), p. 287.
[7]D. Mansuroglu, I. U. Uzun-Kaymak, and I. Rafatov, Phys. Plasmas **24**, 053503 (2017).
[8]Yu. P. Raizer and M. S. Mokrov, Phys. Plasmas **20**, 101604 (2013).
[9]I. Rafatov, Plasma Sources Sci. Technol. **25**, 065014 (2016).
[10]H.-G. Purwins and L. Stollenwerk, Plasma Phys. Controlled Fusion **56**, 123001 (2014).
[11]J. P. Trelles, J. Phys. D: Appl. Phys **49**, 393002 (2016).
[12]M. S. Benilov, Phys. Rev. E **58**, 6480 (1998).
[13]L. Dabringhausen, O. Langenscheidt, S. Lichtenberg, M. Redwitz, and J. Mentel, J. Phys. D: Appl. Phys. **38**, 3128 (2005).
[14]A. Bergner, M. Westermeier, C. Ruhrmann, P. Awakowicz, and J. Mentel, J. Phys. D: Appl. Phys. **44**, 505203 (2011).
[15]P. G. C. Almeida, M. S. Benilov, M. D. Cunha, and J. G. L. Gomes, Plasma Sources Sci. Technol. **22**, 012002 (2013).
[16]M. Schmidt, H. Schneidenbach, and M. Kettlitz, J. Phys. D: Appl. Phys. **46**, 435202 (2013).
[17]M. S. Benilov, J. Phys. D: Appl. Phys. **41**, 144001 (2008).
[18]J. Mentel, J. Phys. D: Appl. Phys. **51**, 033002 (2018).
[19]M. S. Benilov, J. Phys. D: Appl. Phys. **40**, 1376 (2007).
[20]M. S. Benilov and M. J. Faria, J. Phys. D: Appl. Phys. **40**, 5083 (2007).
[21]M. S. Benilov, M. D. Cunha, and M. J. Faria, J. Phys. D: Appl. Phys. **42**, 145205 (2009).
[22]R. Bötticher, W. Graser, and A. Kloss, J. Phys. D: Appl. Phys. **37**, 55 (2004).
[23]R. Bötticher and M. Kettlitz, J. Phys. D: Appl. Phys. **39**, 2715 (2006).
[24]P. G. C. Almeida, M. S. Benilov, and M. D. Cunha, J. Phys. D: Appl. Phys. **41**, 144004 (2008).
[25]C. Wang, W. Li, X. Zhang, M. Liao, J. Zha, and W. Xia, IEEE Trans. Plasma Sci. **43**, 3716 (2015).
[26]M. S. Bieniek, P. G. C. Almeida, and M. S. Benilov, J. Phys. D: Appl. Phys. **49**, 105201 (2016).
[27]W. Zhu, P. Niraula, P. G. C. Almeida, M. S. Benilov, and D. F. N. Santos, Plasma Sources Sci. Technol. **23**, 054012 (2014).
[28]W. Zhu and N. Ike, private communication (2017).
[29]P. G. C. Almeida, M. S. Benilov, and M. J. Faria, J. Phys. D: Appl. Phys. **44**, 415203 (2011).
[30]V. N. Melekhin and N. Yu. Naumov, Sov. Phys. Tech. Phys. **29**, 888 (1984).
[31]A. V. Phelps, Z. Lj. Petrović, and B. M. Jelenković, Phys. Rev. E **47**, 2825 (1993).
[32]I. D. Kaganovich, M. A. Fedotov, and L. D. Tsendin, Tech. Phys. **39**, 241 (1994).
[33]K. H. Schoenbach, M. Moselhy, and W. Shi, Plasma Sources Sci. Technol. **13**, 177 (2004).
[34]M. Moselhy and K. H. Schoenbach, J. Appl. Phys. **95**, 1642 (2004).
[35]Yu. D. Korolev and K. H. Schoenbach, in *Proceedings of the XXVII ICPIG*, Eindhoven, the Netherlands, edited by E. M. van Veldhuizen (Eindhoven University of Technology, Eindhoven, 2005).
[36]N. Takano and K. H. Schoenbach, in *Abstracts of the 2006 IEEE International Conference on Plasma Science* (IEEE, Traverse City, MI, USA, 2006), p. 247.
[37]B.-J. Lee, H. Rahaman, K. Frank, L. Mares, and D.-L. Biborosch, in *Proceedings of the 28th ICPIG*, Prague, edited by J. Schmidt, M. Šimek, S. Pekárek, and V. Prukner (Institute of Plasma Physics AS CR, Prague, 2007), pp. 900–902.
[38]B.-J. Lee, D.-L. Biborosch, K. Frank, and L. Mares, J. Optoelectron. Adv. Mater. **10**, 1972 (2008).
[39]K. H. Schoenbach and W. Zhu, IEEE J. Quantum. Electron. **48**, 768 (2012).
[40]W. Zhu and P. Niraula, Plasma Sources Sci. Technol. **23**, 054011 (2014).
[41]M. S. Bieniek, P. G. C. Almeida, M. S. Benilov, W. Zhu, and P. Niraula, in *43rd IEEE International Conference on Plasma Science* (*ICOPS 2016*) (2016).
[42]W. Zhu and P. Niraula, private communication (2014).
[43]P. G. C. Almeida and M. S. Benilov, Phys. Plasmas **20**, 101613 (2013).
[44]P. G. C. Almeida, M. S. Benilov, and M. J. Faria, IEEE Trans. Plasma Sci. **39**, 2190 (2011).
[45]P. G. C. Almeida, M. S. Benilov, and M. J. Faria, Plasma Sources Sci. Technol. **19**, 025019 (2010).
[46]G. J. M. Hagelaar, F. J. de Hoog, and G. M. W. Kroesen, Phys. Rev. E **62**, 1452 (2000).
[47]A. Salabas, G. Gousset, and L. L. Alves, Plasma Sources Sci. Technol. **11**, 448 (2002).
[48]Yu. P. Raizer, *Gas Discharge Physics* (Springer, Berlin, 1991).